Optimal Scheduling and Beamforming in Relay Networks with Energy Harvesting Constraints

Shimin Gong*, Lingjie Duan*, Natarajan Gautam†

*ESD Pillar, Singapore University of Technology and Design

†Dept. of Industrial and Systems Engineering, Texas A&M University

Abstract

In this paper, multiple relays capable of harvesting energy from radio-frequency (RF) signals are employed to collaboratively forward data from a source transmitter to its destined receiver. Due to the relays' inability to harvest energy and transmit data simultaneously, the source needs to optimally schedule the relays' energy harvesting (EH) and data transmission. Considering different channel conditions and energy constraints, the relays need to optimally design a beamforming vector that specifies each relay a power amplifier coefficient to forward the source signal and suppress the noise. By joint EH scheduling and beamforming, we maximize the overall throughput formulated in a non-convex problem. We first propose a centralized scheme that achieves the optimal throughput by exploiting the monotonicity in the problem structure. We further propose a distributed sub-optimal scheme in a game theoretic approach, which requires the source and the relays to iteratively update EH scheduling and beamforming vector, respectively. We show that the sub-optimal scheme has a threshold-based structure for the relays' power control depending on the source-relay channel conditions. Numerical results show near-optimal performance of the distributed scheme compared with the centralized optimal scheme.

Index Terms

Relay beamforming, energy harvesting, potential game, monotonic optimization

I. Introduction

Recently, wireless energy harvesting (EH) provides a low-cost and sustainable way to keep network connectivity for battery-powered wireless devices, which traditionally require periodic replacement or recharging of batteries. It allows wireless devices to harvest energy from ambient

environment (e.g., solar, wind, and radio frequency (RF) signals) to power wireless information transmissions (e.g., [1] and [2]). Despite low cost, EH has its difficulty to be widely deployed in wireless communications. Compared with battery or on-grid power supply, EH is intermittent in nature and the harvested energy is random due to the dynamics of ambient environment.

The randomness in EH imposes additional constraints on wireless users' energy consumptions for communications, therefore requires novel architecture design and energy management for EH systems. Relying on energy storage, a prominent harvest-store-use (HSU) architecture [3] is proposed to stabilize the energy supply for data transmission over time. A practical finite energy buffer is studied in [4] where the authors proposed an adaptive power allocation scheme to maximize network throughput with a time deadline constraint. This work has been extended to the cases with Gaussian relay channel in [5], non-ideal transmitter model in [6], multiple batteries in [7], hybrid and time-correlated EH in [8] and [9], respectively. Despite such advances, the HSU architecture is still difficult to be used for industry. Firstly, it requires complicated and costly circuit design to assist frequent switching between battery charging and discharging. For example, the charging of Lithium batteries requires a high pulsating charging current, which usually relies on an auxiliary battery or a charging circuit [2]. Secondly, the offline optimal energy management strategies require the non-causal information about energy and data arrivals, leading to a theoretical investigation on the performance upper bound, e.g., [3]–[5]. Though some other works focus on online energy management strategies with causal information, they are sub-optimal to the offline strategies and usually require known statistical information about the energy arrivals [10]. For example, the authors in [8] designed the online strategy in a stochastic dynamic program approach, requiring known probability distribution functions of the channel gain, harvested energy, and the incoming data bits. The authors in [6] assumed that the energy arrival follows a compound Poisson process with known mean value and the distribution of harvested energy in each arrival is also known.

Another approach to tackle the randomness in EH relies on cooperation among individual EH devices. In a distributed wireless network, the EH profiles (e.g., the EH rates) at different devices are time varying and location dependent. Hence, cooperative communications may provide a network-level solution to balance the use of harvested energy in different EH devices. To this end, relaying protocols have been proposed in [11], where a relay can harvest energy from the transmitter and use the harvested energy to forward the source information to its destination, in

either a time switching or power splitting protocol. In [12], the authors examined different power splitting strategies in a multi-access model, where the relay can harvest energy from multiple transceiver pairs and split the harvested energy for relaying the traffic of different transceiver pairs. In [13], the harvested energy can transfer bidirectionally between the source and the relay in order to maximize the sum throughput. When there are multiple EH relays, optimal relay selection has been studied in [14] and [15], and an asymptotic network performance has been analyzed in [16] with an increasing number of EH relays.

However, most of the existing works either study a single relay model (e.g., [11]–[13]), or selecting single relay from a set of candidates (e.g., [14]–[16]). In fact, the amount of harvested energy at single node is typically small and insufficient to sustain wireless transmissions [17]. Hence, a single relay may not ensure desired quality of service at the receiver. To this end, we are interested in selecting multiple EH relays to enhance the reliability of information reception. By the relays' collaborative power control, we can create constructive multipath effect at the destined receiver and weaken the signal strength at undesired directions, and thus improve data rate at the receiver far away from the source transmitter. However, due to different channel conditions from the relays to the receiver, it may not be optimal for all the relays to transmit with the highest power (e.g., [18], [19]). Intuitively, a better performance can be obtained by decreasing the transmit power of some relays with bad channel conditions.

Moreover, we consider a novel easy-to-implement harvest-use (HU) architecture without costly energy storage system like rechargeable batteries and complicated energy management at the relays. Instead, the HU architecture relies on super-capacitors to store the harvested energy [1]. Compared with the rechargeable batteries, the super-capacitors have much larger recharge cycles (i.e., theoretically infinite and more than one million practically), high charge and discharge efficiency at small energy levels, which make super-capacitors suitable for EH from low RF signals. In another aspect, the super-capacitors have lower energy/power density and higher self-discharge rate, which means that the stored energy is leaking out at a faster rate than the rechargeable batteries. These characteristics make the HU architecture suitable for deployment in a wireless sensor network where nodes keep silent most of the time and exchange bursty short messages randomly. Within this scenario, the EH devices have the motivation to deplete all their energy to maximize the instant data rate, otherwise the remaining energy will be leaking out during the inter-transmission periods. A similar HU architecture has been proposed in [20]

where single EH relay is employed to enhance the overall throughput in a two-hop network, by always transmitting with its peak power.

In this work, we consider multiple EH relays collaboratively forwarding the source signal in a half-duplex mode. We aim to determine the relays' optimal strategy to maximize the throughput in each transmission period. Note that a better relay in terms of channel condition may not harvest sufficient energy, so the relays' transmission control has to take account of both the relays' channel conditions and EH profiles. Specifically, our main contributions are summarized as follows:

1) *The HU architecture for EH relay system:* We consider a novel HU architecture to power cooperative communications, where multiple relays can harvest energy from RF signals and forward the source signal to enhance the throughput at the receiver. Due to the relays' inability to harvest and transmit simultaneously, we optimally schedule the data transmissions according to the relays' EH profiles and the channel conditions in both the source-relay and relay-destination channels.
2) *Optimal EH scheduling and relay beamforming:* We allow each relay to choose a distinct power amplifier coefficient and formulate the throughput maximization as a non-convex optimization problem with joint EH scheduling at the source and beamforming at the relays. By exploiting monotonicity of the problem, we propose a centralized algorithm that achieves the global optimum through successive approximation.
3) *Distributed source-relay update scheme:* We also propose a sub-optimal scheme that distributes the computing task to both the source and the relays. The source firstly chooses and informs the relays an EH scheduling decision, then individual relays distributively update their beamforming vector in a potential game with guaranteed convergence to Nash equilibrium, which in return guides the source to update EH scheduling decision. This source-relay update process is shown to achieve near-optimal performance.
4) *Interplay between relays' EH and channel conditions:* When the relays have good channel conditions, the relays' EH profile becomes the bottleneck and dominates the throughput performance. In this case, at least one relay should transmit at peak power to fully make use of the harvested energy. When the channel conditions are not desirable, it is preferable to reduce the number of relays or their transmit power to suppress the noise at the receiver. Therefore, the optimization of the relays' transmit power needs to balance between both

aspects, achieving the optimal throughput performance.

The rest of this paper is organized as follows. In Section II, we introduce the system model and problem formulation. We present a centralized successive approximation in Section III that achieves the global optimum, and propose a sub-optimal scheme in a distributed way in Section IV. We show numerical results in Section V and draw the conclusions in Section VI.

II. System Model and Problem Formulation

We consider a relay network including one source, one destined receiver, and N relays in between denoted by a set $\mathcal{N} = \{1, 2, \ldots, N\}$. Each relay is amounted with single antenna which can be used for transmission and reception in a half-duplex manner. This model can be envisioned as a wireless sensor network deployed in manufactory or buildings where the sensors in different locations monitor malfunctionings or structural faults. The sensors are required to feed back sensing results to a fusion center. To keep a low energy consumption, the sensors operate in an event-driven manner [21], i.e., they stay in a sleep mode most of the time and return to active data transmission when something unusual is detected. In this case, the inter-transmission time can be very long and unpredictable by the sensors.

Due to a large number of sensors and the complex monitoring environment (e.g., some sensors may be embedded inside the machines or buildings), these sensors are designed to sustain themselves by harvesting energy from ambient environment, e.g., the mechanical, thermal, solar energy, or RF signals. Among all these EH techniques, harvesting energy from RF signals has less restrictions on the hardware implementation and is easy to control, i.e., a dedicated RF source can be deployed to transfer power to all sensors simultaneously if ambient RF signals are not strong enough to power up the sensors' data transmissions. Noting that the sensors' inter-transmission time can be long, the stored energy in super-capacitors will be depleting due to the super-capacitors' high self-discharge rate.

A direct link between a sensor and the fusion center may be weak due to a long transmission distance or limited transmit power at the sensor. Therefore, a sensor requires the neighboring sensors to relay its data to the fusion center. An example of 3 relays is illustrated in Fig. 1. Let h_n and g_n denote the channel coefficients from the source to relay n and from relay n to the destination, respectively, for any $n \in \mathcal{N}$. Besides, h_n and g_n are prior information and can be obtained through channel estimation at the relays and the destination, respectively.

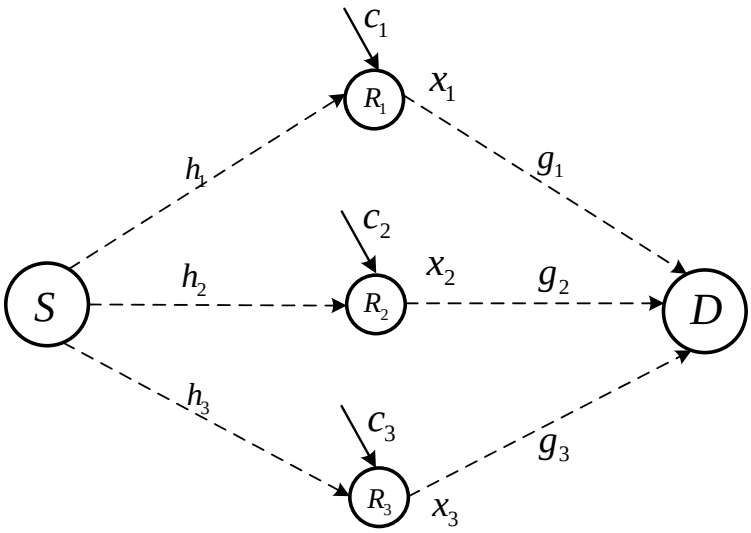

Fig. 1: Two hop relay model.

A. Source's EH Scheduling

We assume that each node is capable of harvesting energy from the RF signal, which relies on the same antenna used for signal reception. The harvested energy is stored in a super-capacitor, rather than traditional rechargeable battery. However, the current receiver design does not allow direct EH from the information carrier (e.g., [20], [22]), introducing the confliction between EH and information transmission. This confliction can be avoided by a time splitting scheme [22]. Specifically, we organize the data transmissions from the source to the destination in a time-slotted model as shown in Fig. 2. Each time slot is of a unit length within a frame structure and allocated to one relay-assisted data transmission. We assume that all wireless links exhibit frequency non-selective block fading [23], i.e., the channel coefficients remain constant during one frame, and may change independently from one frame to another.

The first part of a time slot $w \in [0, 1]$ is used to charge the relays' super-capacitors by EH from RF signals, while the other part of the time slot $1-w$ is used for the relays' signal receptions and forwarding. Thus, the optimal splitting of a time slot requires a trade-off study between EH and data transmission. We assume the same EH time w for all relays as it is more energy-efficient, otherwise some relay has to wait until the completion of other relays' EH, leading to a waste of harvested energy due to the super-capacitor's high self-discharge rate. The high self-discharge rate also causes energy loss during the EH time w, and hence the equivalent EH rate c_n is the

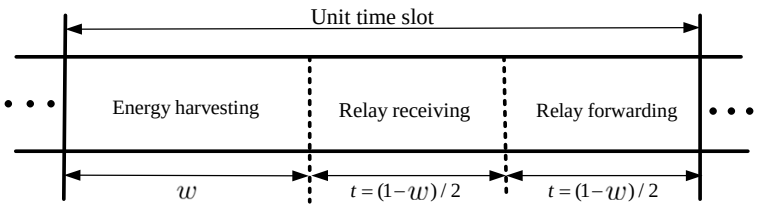

Fig. 2: Time slotted structure.

actual harvesting rate minus the self-discharge rate. Note that c_n depends on the energy density or spectrum environment at specific location. It is assumed as a known constant at the beginning of each time slot. This assumption is reasonable as the strength of ambient RF signals changes in a much larger time scale than the time slot for data transmissions (e.g., [7], [24]). In the remaining part of a time slot, the source first broadcasts a data packet to all the relays, then each relay forwards the data to the destination concurrently. The channel time can also be optimally scheduled for the relays to receive and forward the source signal as studied in [25] and [26]. In this paper, for ease of synchronization, we equally divide the channel time into two intervals with equal length $t = \frac{1-w}{2} \in [0, 1/2]$, similar to the works in [11] and [12].

B. Relays' Power Control

Given the EH time w, the total harvested energy at relay n is given by $E_n = c_n w$ and the peak transmit power[1] is given as follows:

$$p_n = \frac{c_n w}{(1-w)/2} = \frac{c_n}{t/(1-2t)}. \tag{1}$$

When the source sends a message s with transmit power p_0, the received message m_n at relay n is $m_n = \sqrt{p_0} h_n s + \sigma_n$, where σ_n is the additive noise at relay n and follows a standard normal distribution with zero mean and unit variance, i.e., $\sigma_n \sim \boldsymbol{N}(0, 1)$. Note that p_0 is also related to the energy harvesting time w and can be chosen optimally in each time slot. However, different choice of p_0 will not affect our problem formulation and the analytical results in this paper. For simplicity, we assume it constant in our problem formulation.

[1]Note that energy consumption in data reception is much smaller than that in data transmission [27]. Thus, we assume it as a constant that offsets the harvested energy in the relay's super-capacitor.

Assuming $\mathbb{E}\big[|s|^2\big] = 1$, the average received signal strength at relay n is $1 + p_0 h_n^2$. Then, relay n forwards the received signal as well as the noise to the destination by using a power amplifier coefficient $x_n\sqrt{\frac{p_n}{1+p_0h_n^2}}$, where $x_n \in [0,1]$ is a normalized power amplifier coefficient such that the relay's transmit power is given as $x_n^2 p_n$. Hence, we define $\boldsymbol{x} = [x_1, x_2, \ldots, x_N]^T$ as the relays' transmit beamforming vector. Through proper transmitter synchronization and phase alignment (e.g., [18], [19]), the amplified signals are combined at the destined receiver as

$$y = \sum_{n=1}^{N} x_n \sqrt{\frac{p_n p_0}{1+p_0 h_n^2}} h_n g_n s + \sum_{n=1}^{N} x_n \sqrt{\frac{p_n}{1+p_0 h_n^2}} g_n \sigma_n + v_d,$$

where $v_d \sim \boldsymbol{N}(0,1)$ is the noise in reception. The first term contains the useful information from the source, while the second term is the amplified noise forwarded by the relays. Depending on EH time w and power control parameter x_n at each relay $n \in \mathcal{N}$, the signal-to-noise ratio (SNR) at the destined receiver can be found as

$$\gamma = p_0 \left(\sum_{n=1}^{N} \frac{x_n g_n h_n \sqrt{p_n}}{\sqrt{1+p_0 h_n^2}} \right)^2 \Big/ \left(1 + \sum_{n=1}^{N} \frac{x_n^2 g_n^2 p_n}{1+p_0 h_n^2} \right). \tag{2}$$

C. Problem Formulation for Throughput Maximization

Given the relays' channel information and EH rates, our objective is to maximize the throughput in the current time slot, i.e., $r(t, \boldsymbol{x}) = t \log\left(1 + \gamma(t, \boldsymbol{x})\right)$, by jointly choosing the EH time w (or the transmission time $t = \frac{1-w}{2} < \frac{1}{2}$) and the relays' beamforming vector $\boldsymbol{x}$. The optimization of the transmit power p_0 at the source node can be performed in a one-dimensional search. Specifically, the source node can firstly fix p_0 and find the optimal EH time w by solving the problem $\max_{t,\boldsymbol{x}} r(t, \boldsymbol{x})$. Given this EH time w and the EH rate c_0 at the source node, it can anticipate the amount of energy (i.e., $c_0 w$) available for data transmission during the time interval $(1-w)/2$. If the harvested energy is enough to support the data transmission, i.e., $c_0 w > p_0(1-w)/2$, the source node can further increase the transmit power otherwise decrease it in a bisection method. Due to the simplicity of this bisection method, we did not consider the optimization of p_0 in this work. Instead, we focus on the optimization problem $\max_{t,\boldsymbol{x}} r(t, \boldsymbol{x})$ in each iteration with a fixed transmit power p_0 at the source node. Without loss of generality, we normalize $p_0 = 1$ in the problem formulation and define two constants to assist our discussions

as follows:

$$\boldsymbol{a} = \left[\frac{g_1 h_1\sqrt{c_1}}{\sqrt{1+h_1^2}}, \frac{g_2 h_2\sqrt{c_2}}{\sqrt{1+h_2^2}}, \ldots, \frac{g_N h_N\sqrt{c_N}}{\sqrt{1+h_N^2}}\right]^T, \tag{3a}$$

$$\boldsymbol{b} = \text{diag}\left(\left[\frac{g_1\sqrt{c_1}}{\sqrt{1+h_1^2}}, \frac{g_2\sqrt{c_2}}{\sqrt{1+h_2^2}}, \ldots, \frac{g_N\sqrt{c_N}}{\sqrt{1+h_N^2}}\right]\right), \tag{3b}$$

where $\text{diag}(\cdot)$ denotes a diagonal matrix with diagonal element specified by a given row vector. Let $A = \boldsymbol{a}\boldsymbol{a}^T$ and $B = \boldsymbol{b}\boldsymbol{b}^T$, by substituting the peak power (1) into (2), the SNR at the destination node is now given by

$$\gamma(t, \boldsymbol{x}) = \frac{\boldsymbol{x}^T A \boldsymbol{x}}{f(t) + \boldsymbol{x}^T B \boldsymbol{x}}, \tag{4}$$

where $f(t) = t/(1-2t) = t/w$ represents the equivalent background noise level, which varies with different choices of EH time w. Note that, the objective $r(t, \boldsymbol{x})$ defines a complicated non-concave function of t and $\boldsymbol{x}$, and is difficult to achieve its maximum in general. However, by change of variable, we easily find that $r(t, \gamma) = t\log(1+\gamma)$ is an increasing function of t and γ, which is an appealing property for the design of a global optimal algorithm in next section.

The monotonicity of $r(t, \gamma)$ with respect to t and γ allows us to simplify the throughput maximization problem as follows:

$$\max_{t,\gamma}\{r(t, \gamma) : (t, \gamma) \in \Omega\}, \tag{5}$$

where Ω defines the feasible set of (t, γ):

$$\Omega = \left\{(t, \gamma)\middle|\ 0 \le \gamma \le \tfrac{\boldsymbol{x}^T A \boldsymbol{x}}{f(t)+\boldsymbol{x}^T B \boldsymbol{x}}, \forall\, t \in [0, \tfrac{1}{2}), \boldsymbol{x} \in [\boldsymbol{0}, \boldsymbol{1}]\ \right\}. \tag{6}$$

The monotonicity of the objective in (5) implies that the global optimum will be achieved on the boundary of its feasible set Ω. To locate the optimal solution (t^*, γ^*), we investigate the following property of Ω that motivates the development of the monotonic optimization method.

Definition 1: A set Ω is normal if $\boldsymbol{z}' \in \Omega$ for all $0 \preceq {}^2\boldsymbol{z}' \preceq \boldsymbol{z}$ and $\boldsymbol{z} \in \Omega$. A point $\boldsymbol{z} \in \Omega$ is an upper boundary point if $\boldsymbol{z}' \notin \Omega$ for any $\boldsymbol{z}' \succeq \boldsymbol{z}$ and $\boldsymbol{z}' \neq \boldsymbol{z}$. The set of upper boundary point of Ω is denoted by $\overline{\Omega}$.

Lemma 1: The feasible set Ω defined in (6) is normal and the optimum of (5) is achieved on its upper boundary set $\overline{\Omega}$.

The proof of Lemma 1 is given in Appendix A.

[2]Here $\boldsymbol{z}' \preceq \boldsymbol{z}$ means that $\boldsymbol{z} - \boldsymbol{z}'$ has non-negative entries.

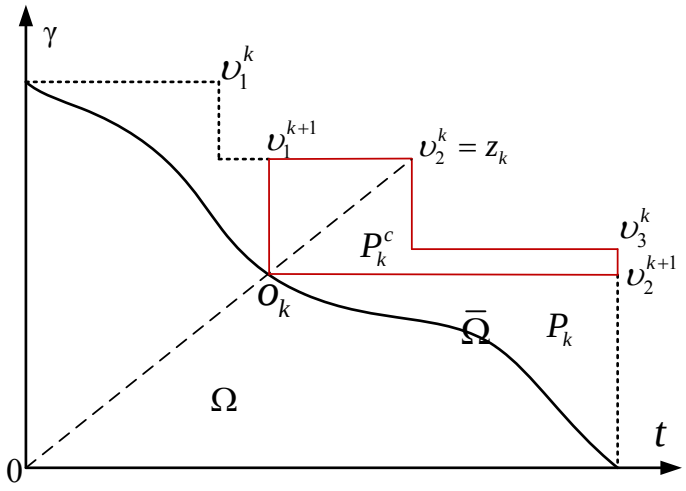

Fig. 3: Polyblock approximation.

III. Centralized EH Scheduling and Power Control

The basic idea of monotonic optimization [28] is to successively approximate the feasible set Ω by generating *regularly shaped* normal sets (i.e., polyblocks P_k) such that $P_0 \supset P_1 \supset \cdots \supset P_k \supset \cdots \supset \Omega$, starting from an initial polyblock P_0. Note that set Ω can be viewed as the union of infinitely many *boxes* in the form of $[\mathbf{0}, \boldsymbol{v}]$ where $\boldsymbol{v}$ is the vertex of a box set. The construction of polyblock P_k is to approximate Ω by a *finite set* of boxes as illustrated in Fig. 3. In the k-th iteration, the algorithm firstly determines an upper bound r_k^U of the global optimum, i.e., $r_k^U = \max_{\boldsymbol{z}=(t,\gamma)\in P_k} r(\boldsymbol{z})$, which will be achieved on one of the vertices of P_k due to the monotonicity of the objective function $r(\cdot)$. Then it updates a lower bound r_k^L by evaluating the objective function at one feasible point o_k on the upper boundary $\overline{\Omega}$. The algorithm ends until the upper and lower bounds converge to the same level within an acceptable error distance ϵ.

A. Update of Upper and Lower Throughput Bounds

Let V_k denote the vertex set of polyblock P_k, the upper bound r_k^U can be easily assessed on the vertices $\boldsymbol{v} \in V_k$ according to the monotonicity of $r(t, \gamma)$. Let $\boldsymbol{z}_k = \arg\max_{\boldsymbol{v}\in V_k} r(\boldsymbol{v})$, then $r_k^U = r(\boldsymbol{z}_k)$ is an upper bound of the optimum r^*. To determine the lower bound r_k^L, we project $\boldsymbol{z}_k$ onto the upper boundary $\overline{\Omega}$ as illustrated in Fig. 3. The projection point $\boldsymbol{o}_k$ is the intersection between the upper boundary $\overline{\Omega}$ and a straight line from $\boldsymbol{z}_k$ to the origin $\mathbf{0}$. Then we can evaluate

the lower bound as $r_k^L = r(\boldsymbol{o}_k)$. Note that $\boldsymbol{o}_k$ is a scaled version of $\boldsymbol{z}_k$. Let $\boldsymbol{o}_k = s_k \boldsymbol{z}_k$ and the scaling factor s_k is obtained by

$$s_k = \max_s \{s \mid s\boldsymbol{z}_k \in \Omega\}. \tag{7}$$

That is, we need to find the maximum scaling factor s_k such that $\boldsymbol{o}_k(s_k) \triangleq s_k \boldsymbol{z}_k$ belongs to set $\overline{\Omega}$. Since Ω is a normal set, it is easy to verify that $\boldsymbol{o}_k(s) \notin \Omega$ for any $s_k < s \leq 1$ and $\boldsymbol{o}_k(s) \in \Omega$ for any $0 \leq s \leq s_k$, which suggests a bisection method to pinpoint the value of s_k. In each iteration of the bisection method, checking $\boldsymbol{o}_k(s) \in \Omega$ with fixed scaling factor s is equivalent to find a solution $\boldsymbol{x} \in [\mathbf{0}, \mathbf{1}]$ such that $s\gamma_k \leq \frac{\boldsymbol{x}^T A \boldsymbol{x}}{f(st_k) + \boldsymbol{x}^T B \boldsymbol{x}}$, that is, $s\gamma_k f(st_k) \leq \boldsymbol{x}^T (A - s\gamma_k B)\boldsymbol{x}$. To check the feasibility of this inequality, we need to solve the following problem

$$p(s, \boldsymbol{z}_k) \triangleq \max_{\boldsymbol{x}} \{\boldsymbol{x}^T (A - s\gamma_k B)\boldsymbol{x} : \mathbf{0} \preceq \boldsymbol{x} \preceq \mathbf{1}\}, \tag{8}$$

and compare the optimum $p(s, \boldsymbol{z}_k)$ with the target threshold $s\gamma_k f(st_k)$. If $p(s, \boldsymbol{z}_k) \geq s\gamma_k f(st_k)$, we have $\boldsymbol{o}_k(s) \in \Omega$ and s will be increased in next iteration.

The availability of $p(s, \boldsymbol{z}_k)$ is essential for finding accurate scaling factor s_k in (7) and ensuring the convergence of the polyblock approximation algorithm. However, maximization of such a quadratic objective in (8) is not straightforward as the matrix coefficient $(A - s\gamma_k B)$ may be indefinite. This makes the maximization problem NP-hard and the feasibility check ambiguous. Fortunately, the polynomial optimization [29] allows us to relax problem (8) to a semi-definite program (SDP). Through successive SDP relaxations, we can achieve the global optimum $p(s, \boldsymbol{z}_k)$ within a few steps. Besides, a well designed branch-and-bound numerical algorithm is presented in [30] that can solve such non-convex problems efficiently.

B. Generation of New Polyblock

If $\boldsymbol{z}_k = \arg\max_{\boldsymbol{v} \in V_k} r(\boldsymbol{v})$ in the k-th iteration happens to be on the upper boundary $\overline{\Omega}$ (i.e., $\boldsymbol{z}_k$ coincides with its projection $\boldsymbol{o}_k \in \overline{\Omega}$ with $s_k = 1$), then $r_k^U = r_k^L$ and $\boldsymbol{z}_k$ is the global optimal solution, otherwise we will update the vertex set V_{k+1} and generate a "smaller" polyblock $P_{k+1} \subset P_k$ to update either a tighter upper or lower bound of r^*. Now assuming $\boldsymbol{z}_k \notin \overline{\Omega}$ as shown in Fig. 3, since Ω is a normal set, we have $\Omega \bigcap P_k^c = \emptyset$ where $P_k^c \triangleq \{\boldsymbol{z} \in P_k \mid \boldsymbol{z} \succeq \boldsymbol{o}_k\}$ denotes, for an instance, the red hexagon in Fig. 3. Hence, the removal of this part P_k^c from polyblock P_k will give a tighter upper bound of r^*.

Moreover, the removal of P_k^c will generate new vertices and help erase some redundant vertices in V_k. We have $\overline{V}_k(\boldsymbol{o}_k) = \{\boldsymbol{v} \in V_k \mid \boldsymbol{v} \succeq \boldsymbol{o}_k\}$ to denote the redundant vertices, e.g., $\overline{V}_k(\boldsymbol{o}_k) = \{\boldsymbol{v}_2^k = \boldsymbol{z}_k, \boldsymbol{v}_3^k\}$ in Fig. 3. To determine the newly generated vertices, we first define the reflection of $\boldsymbol{o}_k$ as $\bar{\boldsymbol{z}}_k$ such that $\bar{\boldsymbol{z}}_k(i) = \max_{\boldsymbol{v} \in \overline{V}_k(\boldsymbol{o}_k)} \boldsymbol{v}(i)$ for $1 \leq i \leq \dim(\boldsymbol{o}_k)$[3], where $\boldsymbol{v}(i)$ and $\bar{\boldsymbol{z}}_k(i)$ denote the i-th entries in $\boldsymbol{v}$ and $\bar{\boldsymbol{z}}_k$, respectively. That is, the i-th entry of $\bar{\boldsymbol{z}}_k$ will take the largest value on the i-th dimension of all vertices $\boldsymbol{v} \in \overline{V}_k(\boldsymbol{o}_k)$. Given this construction of $\bar{\boldsymbol{z}}_k$, we can create a number of $\dim(\boldsymbol{o}_k)$ new vertices each given by $\boldsymbol{v}_j^{k+1} = \boldsymbol{o}_k + \Lambda_j(\bar{\boldsymbol{z}}_k - \boldsymbol{o}_k)$. The square matrix Λ_j has a unique non-zero element equal to 1 on the j-th diagonal entry, and thus the multiplication $\Lambda_j(\bar{\boldsymbol{z}}_k - \boldsymbol{o}_k)$ only keeps the j-th element of vector $\bar{\boldsymbol{z}}_k - \boldsymbol{o}_k$. The new vertex set V_{k+1} will include all newly generated vertices $\boldsymbol{v}_j^{k+1}$ and exclude all redundant vertices in set $\overline{V}_k$. With a little abuse of notation, it is updated as follows:

$$V_{k+1} = V_k - \overline{V}_k + \{\boldsymbol{v}_j^{k+1}\}_{0 \leq j \leq \dim(\boldsymbol{o}_k)}. \tag{9}$$

Once we update V_{k+1}, we can construct new polyblock P_{k+1} as the union of finite boxes.

The detailed steps of successive polyblock approximation are shown in Algorithm 1, where ϵ is an error tolerance ensuring an ϵ-optimal solution $\boldsymbol{z}^* = (t^*, \gamma^*)$ when the algorithm terminates. The vertex of the initial polyblock P_0 can be set to $(1/2, \gamma_{max})$ where γ_{max} denotes the largest possible SNR for any $t \in [0, 1/2]$ and $\boldsymbol{x} \in [\boldsymbol{0}, \boldsymbol{1}]$. Note that $\gamma < \frac{\boldsymbol{x}^T A \boldsymbol{x}}{\boldsymbol{x}^T B \boldsymbol{x}}$ and the maximum of $\frac{\boldsymbol{x}^T A \boldsymbol{x}}{\boldsymbol{x}^T B \boldsymbol{x}}$ is confined by the largest eigenvalue of matrix $B^{-1}A$ [30], therefore we can set $\gamma_{max} = \lambda_{max}(B^{-1}A)$, which only relates to the relays' channel conditions and EH rates. Given the convergent point $\boldsymbol{z}^* = (t^*, \gamma^*)$ in Algorithm 1 and the feasibility region of $\boldsymbol{x} \in [\boldsymbol{0}, \boldsymbol{1}]$, the optimal beamforming vector $\boldsymbol{x}^*$ can be obtained by solving the quadratic equation $\gamma^* f(t^*) = (\boldsymbol{x}^*)^T (A - \gamma^* B)\boldsymbol{x}^*$ in a numerical method (e.g., Newton's method). Moreover, the optimum of problem (8) equals to $\gamma^* f(t^*)$ at the convergence of Algorithm 1, otherwise we will update the projection in step 8 of Algorithm 1. Therefore, the optimal $\boldsymbol{x}^*$ can also be obtained by solving the projection problem (8) with $s\gamma_k$ replaced by γ^*. By calling the same solution method for problem (8) in step 8, we do not need to design additional procedures to solve the equation $\gamma^* f(t^*) = (\boldsymbol{x}^*)^T (A - \gamma^* B)\boldsymbol{x}^*$, and thus reduce the computational complexity of Algorithm 1.

Proposition 1: Algorithm 1 is guaranteed to converge to ϵ-optimal solution in a finite number of iterations for any $\epsilon > 0$.

[3] $\dim(\boldsymbol{o}_k)$ denotes the dimension of $\boldsymbol{o}_k$ and here we have $\dim(\boldsymbol{o}_k) = 2$.

Algorithm 1 Successive Polyblock Approximation

set initial vertex set $V_k = \{(1/2, \gamma_{max})\}$, polyblock P_k, $r_k^U = 1$, and $r_k^L = 0$ for $k = 0$
while $|r_k^U - r_k^L| \geq \epsilon$
  $k \leftarrow k + 1$
  update $\boldsymbol{z}_k = \arg\max_{\boldsymbol{v} \in V_{k-1}} r(\boldsymbol{v})$ and $r_k^U = r(\boldsymbol{z_k})$
  if $\boldsymbol{z}_k \in \Omega$ then
    update $r_k^L = r(\boldsymbol{z}_k)$
  else
    find projection $\boldsymbol{o}_k = s_k \boldsymbol{z}_k \in \overline{\Omega}$
    update $r_k^L = r(\boldsymbol{o}_k)$ if $r(\boldsymbol{o}_k) \geq r_k^L$
    update vertex set V_k by (9)
  end if
end while
set $\boldsymbol{z}^* = \boldsymbol{z}_k$ and $r^* = r(\boldsymbol{z}^*)$
obtain t^* from $\boldsymbol{z}^*$ and $\boldsymbol{x}^*$ by solving problem (8)

This result can be proved similarly as in Proposition 3.9 of [28], by showing the Lipschitz continuity of the objective function $r(t, \gamma)$. We provide the details in Appendix B.

Fig. 4 gives an illustrative example of Algorithm 1. For a fixed transmission time t, we solve the projection problem (8) and obtain the maximum SNR γ. All these numerically calculated points (t, γ) form the upper boundary $\overline{\Omega}$, which is denoted by the dashed line in Fig. 4(a). Observing the shape of curve $\overline{\Omega}$, the feasible region Ω is non-convex but normal. When the generation of polyblocks, denoted by solid lines in Fig. 4(a), becomes closer to the global optimum, denoted by marker "*", the gap between r_k^U and r_k^L is diminishing to a desired accuracy $\epsilon = 10^{-5}$ as shown in Fig. 4(b). The implementation of the successive polyblock approximation method requires a centralized collection and processing of all information about the channel conditions and EH rates at individual relays. Each relay can estimate EH rate c_n and the channel coefficient h_n, and then report them to the receiver. Combined with the channel coefficient g_n, the destined receiver can perform successive polyblock approximation, and feed back the optimal EH scheduling parameter t^* to the source and the optimal beamforming vector $\boldsymbol{x}^*$ to the relays, respectively.

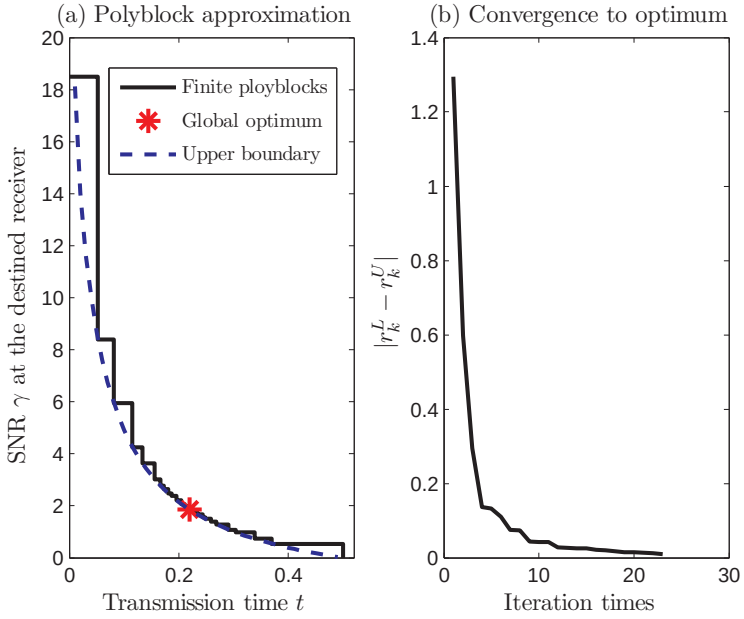

Fig. 4: An illustrative example.

IV. Distributed EH Scheduling and Power Control

The successive polyblock approximation method allocates main computational task to a single device (e.g., the destined receiver), and requires global information about the relays' channel conditions and EH rates. Though it gives a systematical way to assess the optimal throughput performance, we prefer to distribute the whole decision making process to individual devices and each device makes a local decision independently. In this section, we propose a distributed algorithm that requires the interactions between the source and the relays. The idea is to let the source decide the EH scheduling parameter t and the relays locally optimize the beamforming vector $\boldsymbol{x}$, respectively.

A. An Iterative Sub-optimal Method

1) Source updates EH scheduling decision: The following property of the optimal transmission time t helps us design the decision making strategies for the source and the relays.

Lemma 2: The SNR $\gamma(t, \boldsymbol{x})$ is decreasing and the throughput $r(t, \boldsymbol{x})$ is concave with respect to the transmission time t. Hence, the optimal t^* in (5) is achieved interior to its feasible set $[0, 1/2)$ and can be found by solving the first-order optimality condition $\partial r(t, \boldsymbol{x})/\partial t = 0$.

The result is derived by checking the derivative of γ and r with respect to t, respectively. Detailed proof is given in Appendix C. Intuitively, when the source increases EH time w, the relays will harvest more energy and consume it in a shorter transmission time $t = \frac{1-w}{2}$, resulting in a higher SNR at the destination for a fixed beamforming vector $\boldsymbol{x}$. However, the overall throughput may not be necessarily increased since the transmission time t is reduced. Lemma 2 gives the optimality condition for EH scheduling and implies a gradient-based method to search for a local optimal transmission time t^*.

2) Relays update beamforming vector: Given the EH scheduling decision t, the relays then optimize $\boldsymbol{x}^*(t)$ achieving the highest SNR at the destined receiver, i.e.,

$$\boldsymbol{x}^*(t) = \arg \max_{\mathbf{0} \preceq \boldsymbol{x} \preceq \mathbf{1}} \frac{\boldsymbol{x}^T A \boldsymbol{x}}{f(t) + \boldsymbol{x}^T B \boldsymbol{x}}. \tag{10}$$

Let $\gamma(t, \boldsymbol{x}^*(t))$ denote the maximum achievable SNR for a fixed t and we define $\rho \triangleq \gamma(t, \boldsymbol{x}) = \frac{\boldsymbol{x}^T A \boldsymbol{x}}{f(t) + \boldsymbol{x}^T B \boldsymbol{x}} \leq \gamma(t, \boldsymbol{x}^*(t))$, which is a ratio between two convex functions. Thus, problem (10) is non-concave and existing convex optimization techniques (e.g., [31]) do not apply in this case. To address this difficulty, we reshape problem (10) into a subtractive form $S(\boldsymbol{x}, \rho) = \boldsymbol{x}^T A \boldsymbol{x} - \rho \left(f(t) + \boldsymbol{x}^T B \boldsymbol{x} \right)$. From Dinkelback's Theorem in [31], we have the following result.

Lemma 3: For any fixed ρ, let $\boldsymbol{x}_s(\rho)$ denote the solution to

$$\bar{S}(\rho) = \max_{\boldsymbol{x}} \left\{ \, S(\boldsymbol{x}, \rho) : \; \mathbf{0} \preceq \boldsymbol{x} \preceq \mathbf{1} \, \right\}. \tag{11}$$

If there exists $\rho^* \geq 0$ such that $\bar{S}(\rho^*) = 0$, then $\boldsymbol{x}_s(\rho^*)$ is the optimal solution to (10) and we have $\rho^* = \gamma(t, \boldsymbol{x}_s(\rho^*)) = \gamma(t, \boldsymbol{x}^*(t))$.

From Lemma 3, we require to solve $\bar{S}(\rho^*) = 0$ where ρ^* corresponds to the maximum SNR at the destined receiver. We may consider the Newton iteration to search for the solution ρ^*, i.e., we check the value of $\bar{S}(\rho)$ for some ρ and then update ρ if $\bar{S}(\rho) \neq 0$. The Newton iteration requires the calculation of derivative of $\bar{S}(\rho)$ with respect to ρ, which is not easy as $\bar{S}(\rho)$ is the optimum of problem (11). The following property helps simplify the solution process.

Lemma 4: $\bar{S}(\rho)$ is strictly decreasing with respect to ρ and there is unique solution to $\bar{S}(\rho) = 0$.

This property can be verified by showing that $\bar{S}(\rho_1) = S(\boldsymbol{x}_s(\rho_1), \rho_1) > S(\boldsymbol{x}_s(\rho_2), \rho_1) > S(\boldsymbol{x}_s(\rho_2), \rho_2) = \bar{S}(\rho_2)$ for any $\rho_2 > \rho_1 > 0$. Details can be found in [31]. The monotonicity of $\bar{S}(\rho)$ motivates a bisection method to guide the search for ρ^*. In each step, we maximize a non-convex quadratic objective (11), which has the same structure as in (8). Therefore, the SDP relaxation developed in [29] can be well applied to find $\bar{S}(\rho)$ with any fixed ρ.

Algorithm 2 Iterative Update of EH Scheduling at Source and Beamforming Vector at Relays

1: initialize t_k, $\boldsymbol{x}_k$, and $\rho \in [\rho_{min}, \rho_{max}]$
2: while $|\partial r(t,\boldsymbol{x})/\partial \boldsymbol{x}\big|_{(t_k,\boldsymbol{x}_k)}| + |\partial r(t,\boldsymbol{x})/\partial t\big|_{(t_k,\boldsymbol{x}_k)}| \geq \varepsilon$
3: while $|\bar{S}(\rho)| \geq \varepsilon$ and $|\rho_{max} - \rho_{min}| \geq \varepsilon$
4: evaluate $\bar{S}(\rho)$ in a game-theoretic approach
5: if $\bar{S}(\rho) \geq 0$, update $\rho_{min} = \rho$, end if
6: if $\bar{S}(\rho) \leq 0$, update $\rho_{max} = \rho$, end if
7: update $\boldsymbol{x}_k = \boldsymbol{x}_s(\rho)$ and $\rho = \frac{\rho_{min}+\rho_{max}}{2}$
8: end while
9: set $\Delta_t \leftarrow \big|\partial r(t,\boldsymbol{x})/\partial t\big|_{(t_k,\boldsymbol{x}_k)}\big|$
10: update $t_k \leftarrow t_k + \alpha_k \Delta_t$
11: end while
12: return convergent $(t_k, \boldsymbol{x}_k)$

3) Convergence of source-relay iterations: We summarize the solution method in Algorithm 2, in which the source starts the iteration by choosing an EH scheduling parameter t_k, then in lines $3-8$ of the algorithm, the relays determine the beamforming vector $\boldsymbol{x}_s(\rho^*)$ in a bisection method that maximizes the SNR at the destined receiver for fixed t_k. The update of t_k in lines $9-10$ follows a gradient direction where α_k is a proper step-size. Then the algorithm continues to check whether overall throughput can be further improved in line 2 and notifies the relays to update a beamforming vector if the stopping criterion does not hold.

Proposition 2: The iterative Algorithm 2 is guaranteed to converge to a local optimum.

The proof is straightforward as Algorithm 2 mimics a hill climbing algorithm. In each outer iteration, it updates either beamforming vector $\boldsymbol{x}^*(t)$ (in lines $3-8$) or EH scheduling decision t (in lines $9-10$). The process continues to improve the objective $r(t, \boldsymbol{x}^*(t))$ in every iteration until there is no further improvement. Though the objective is a concave function of t, it does not mean that it is jointly concave in variable $(t, \boldsymbol{x})$. Thus, there may exist several local optimums and Algorithm 2 just guarantees convergence to a local optimum.

B. Relays' Power Control in a Game-Theoretic Approach

Given the global information about the relays' EH rates and channel conditions, the successive SDP relaxation [29] provides an efficient way to optimize the relays' beamforming vector $\boldsymbol{x}(t_k)$. To further resolve the computational complexity of an SDP problem, we propose a fully distributed subroutine to perform the task in line 4 of Algorithm 2. The subroutine maximizes $S(\boldsymbol{x}, \rho)$ through an equal participation of individual relays, instead of solving (11) directly in a centralized manner. To proceed, we expand[4] $S(\boldsymbol{x}, \rho) = \sum_{n=1}^{N} x_n^2(a_n^2 - \rho b_n^2) + \sum_{m \neq n} a_n a_m x_n x_m$ where $a_n = \frac{g_n h_n \sqrt{c_n}}{\sqrt{1+h_n^2}}$ and $b_n = \frac{g_n \sqrt{c_n}}{\sqrt{1+h_n^2}}$. Note that $a_n = b_n h_n$, we have

$$S(\boldsymbol{x}, \rho) = \sum_{n=1}^{N} a_n^2 x_n \left(\left(1 - \frac{\rho}{h_n^2}\right) x_n + \sum_{m=1, m \neq n}^{N} \frac{a_m}{a_n} x_m \right). \tag{12}$$

At this point, we consider decomposing the maximization of $S(\boldsymbol{x}, \rho)$ into N local problems at individual relays. Each relay $n \in \mathcal{N}$ optimizes its own power amplifier coefficient x_n, given the other relays' decision strategies.

1) A potential game modeling: Considering a game-theoretic framework to design the distributed algorithm, we start with three key elements of the game: players, strategies, and payoffs, denoted in a triplet $\mathcal{G} = (\mathcal{N}, \{X_n\}_n, \{u_n\}_n)$. The set of relays $\mathcal{N}$ can be viewed as the players in game $\mathcal{G}$ and the strategy of relay n is to choose a power control parameter x_n from its strategy space $X_n = [0, 1]$, given the other relays' decision vector $\boldsymbol{x}_{-n} \triangleq [x_1, \ldots, x_{n-1}, x_{n+1}, \ldots, x_N]^T$. All relays' decisions constitute the strategy profile $\boldsymbol{x} = [x_1, x_2, \ldots, x_N]^T$. A proper design of the relay's payoff function $u_n(x_n, \boldsymbol{x}_{-n})$ will ensure the convergence to *Nash equilibrium*, in which no relay can further increase its payoff by unilaterally deviating to any other strategies.

One possibility to ensure the existence of Nash equilibrium is to devise a global *potential function* for the relays' payoff $u_n(x_n, \boldsymbol{x}_{-n})$, enforcing $\mathcal{G}$ to be a potential game [32] in which any change of a relay's payoff function will be reflected by the change of the potential function. Therefore, we can set the potential function exactly as $S(\boldsymbol{x}, \rho)$ and maximize it when the game $\mathcal{G}$ achieves Nash equilibrium. Moreover, we have an *exact potential game* (EPG) if any change of a relay's payoff equals the change of the potential function, i.e., $S(x_n, \boldsymbol{x}_{-n}, \rho) - S(\bar{x}_n, \boldsymbol{x}_{-n}, \rho) = u_n(x_n, \boldsymbol{x}_{-n}) - u_n(\bar{x}_n, \boldsymbol{x}_{-n})$, where relay n changes its strategy from x_n to $\bar{x}_n$ and other relays' strategies $\boldsymbol{x}_{-n}$ are unaltered. Given this relationship, we have the following result:

[4]Note that $S(\boldsymbol{x}, \rho) = \boldsymbol{x}^T(A - \rho B)\boldsymbol{x} - \rho f(t)$. We only consider the first term $\boldsymbol{x}^T(A - \rho B)\boldsymbol{x}$ as the other term $\rho f(t)$ is fixed.

Proposition 3: Define the payoff of relay n as follows:

$$u_n(x_n, \boldsymbol{x}_{-n}) = a_n^2 x_n \left(\left(1 - \frac{\rho}{h_n^2} \right) x_n + 2 \sum_{m=1, m \neq n}^{N} \frac{a_m}{a_n} x_m \right), \tag{13}$$

then $\mathcal{G}$ is an EPG with the potential function $S(\boldsymbol{x}, \rho)$ given in (12), and the existence of Nash equilibrium is guaranteed.

The proof is given in Appendix D. The local objective $u_n(x_n, \boldsymbol{x}_{-n})$ is quadratic in the local decision variable x_n. The optimal strategy can be calculated efficiently at individual relays and we summarize the solution as follows.

Proposition 4: Let $x_n^*(\boldsymbol{x}_{-n})$ denote the best response strategy of relay n that maximizes its objective $u_n(x_n, \boldsymbol{x}_{-n})$ given the other relays' strategy profile $\boldsymbol{x}_{-n}$, then

$$x_n^*(\boldsymbol{x}_{-n}) = \begin{cases} 1, & \rho \leq h_n^2 \\ \min\left(1, \frac{\sum_{m=1, m \neq n}^{N} a_m x_m}{a_n(\rho / h_n^2 - 1)}\right), & \rho > h_n^2 \end{cases}. \tag{14}$$

The result is derived by maximizing the payoff function in (13). When $\rho \leq h_n^2$, the payoff $u_n(x_n, \boldsymbol{x}_{-n})$ is an increasing function of x_n, thus $x_n = 1$ is optimal. When $\rho \geq h_n^2$, it is concave on $[0, 1]$. By taking the derivative of $u_n(x_n, \boldsymbol{x}_{-n})$ with respect to x_n and setting it to zero, we obtain the optimal solution $x_n^*(\boldsymbol{x}_{-n})$ in (14).

2) Convergence to Nash equilibrium: In potential game $\mathcal{G}$, Nash equilibrium can be achieved in an iterative manner by individual relays' sequential updates of their best response strategies [32]. Let $\boldsymbol{X} = (\boldsymbol{x}^0, \boldsymbol{x}^1, \cdots)$ be a sequence of strategy profiles generated by the relays' best response updates. Then, the sequence $\boldsymbol{X}$ constitutes an improvement path in which every two consecutive strategy profiles differ in one coordinate, e.g., $\boldsymbol{x}^k$ and $\boldsymbol{x}^{k+1}$ differ in relay n_k's strategy and $u_{n_k}(x_{n_k}^k, \boldsymbol{x}_{-n_k}^k) < u_{n_k}(x_{n_k}^{k+1}, \boldsymbol{x}_{-n_k}^k)$. Note from [32] that, any improvement path is finite for a potential game with discrete strategy space and finite potential function. However, for the game $\mathcal{G}$ with a compact strategy space X_n, the improvement path may be long as the relays' strategy updates may contribute little to improve the potential function. In practice, we have two ways to handle this. Firstly, we can discretize the strategy space X_n into finite power control levels and then follow a finite improvement path to achieve Nash equilibrium. Secondly, we impose the best response updates with an ϵ-stopping condition, which prevents the relays from updating strategies unless they have at least ϵ payoff improvement.

3) Properties of the relays' beamforming vector: The best response strategy in (14) shows that we have a threshold-based policy to choose the relays, depending on the source-relay channel coefficient h_n. A relay n with a good channel gain (i.e., $h_n^2 > \rho$) is chosen to transmit with peak power (i.e., $x_n = 1$), while the other relays with relatively bad channel gain only partially use their harvested energy. An intuitive explanation for this result is that, each relay has two ways to affect the transmission. It not only forwards useful signal but the noise as well. When channel condition is not good and a great noise is received in the source-relay hop, the relay should reduce its transmit power to suppress the noise at the destination. The value of power control parameter x_n is not only decided by EH rates and channel conditions in the source-relay hop, but also influenced by the channel conditions in the relay-destination hop. Moreover, the relays' power control parameters are coupled with each other and cannot be obtained in a closed-form. To shed some light on the implication of Proposition 4, we consider a simple case with two relays and analyze its Nash equilibrium.

Proposition 5: In game $\mathcal{G}$ with 2 relays and let $h_1^2 \geq h_2^2$, we have the following statements:

1) If $\rho \leq h_n^2$ for $n \in \{1, 2\}$, then $\boldsymbol{x} = (1, 1)$ is the unique Nash equilibrium.
2) If $\rho > h_n^2$ for $n \in \{1, 2\}$, then we have a unique Nash equilibrium at $\boldsymbol{x} = (0, 0)$ when $\rho > h_1^2 + h_2^2$, and at $\boldsymbol{x} = (1, 1)$ when $\rho < h_1^2 + h_2^2$.
3) If $h_1^2 \geq \rho > h_2^2$, we have a unique Nash equilibrium at $\boldsymbol{x} = (1, \beta_2 a_1)$ when $\rho \geq \left(1 + \frac{a_1}{a_2}\right) h_2^2$, and at $(1, 1)$ when $\rho < \left(1 + \frac{a_1}{a_2}\right) h_2^2$, where $\beta_n = \frac{h_n^2}{a_n(\rho - h_n^2)}$.

The results in Proposition 5 can be easily extended to the case with more relays. Detailed analysis is given in Appendix E. From Proposition 5, we have two interesting observations:

- When both relays have bad source-relay channels, i.e., $\rho > h_1^2 + h_2^2$, they will not forward data packets to the destination, i.e., $x_1 = x_2 = 0$. This case can happen when the relays are far away from the source.
- When the source-relay channels are good, i.e., $\rho < h_1^2 + h_2^2$, there will be at least one relay transmitting at its peak power. For example in case 3) of Proposition 5, the relay 1 with better channel (e.g., $h_1^2 \geq \rho > h_2^2$) decides $x_1 = 1$ no matter $\rho \geq \left(1 + \frac{a_1}{a_2}\right) h_2^2$ or not.

By this simple case with two relays, we can analyze how the power control parameters x_n change with respect to the relay-destination channel gain g_n. Considering case 3) in Proposition 5 where

Nash equilibrium $(1, \beta_2 a_1)$ is achieved when $h_1^2 \geq \rho > \left(1 + \frac{a_1}{a_2}\right) h_2^2$. Then we have,

$$x_2 = \beta_2 a_1 = \frac{a_1 h_2^2}{a_2(\rho - h_2^2)} = \frac{g_1 h_1 h_2 \sqrt{c_1(1+h_2^2)}}{g_2(\rho - h_2^2)\sqrt{c_2(1+h_1^2)}},$$

which becomes larger/smaller when the relay-destination channel is getting worse/better. This result seems counter-intuition, but we can show that x_2 actually maximizes the difference between the strength of useful signal (i.e., $\boldsymbol{x}^T A \boldsymbol{x}$) and the weighted noise power $\rho(f(t) + \boldsymbol{x}^T B \boldsymbol{x})$. By the construction of the potential function in (12), we have $S((1, x_2), \rho) = -\left(\frac{a_2}{a_1}\right)^2 \left(\frac{\rho - h_2^2}{h_2^2}\right) x_2^2 + 2\left(\frac{a_2}{a_1}\right) x_2 + \frac{h_1^2 - \rho}{h_1^2}$. Take the derivative of $S((1, x_2), \rho)$ with respect to x_2 and set it to zero, the optimum of $S((1, x_2), \rho)$ is achieved when $x_2 = \beta_2 a_1$.

The computational complexity of Algorithm 1 mainly lies in the projection problem in line 8, which can be reformulated in an SDP problem. An SDP can be readily solved by an interior-point method and the analysis of its computational complexity can be found in [33]. The computational complexity of Algorithm 2 mainly lies in the evaluation of $\bar{S}(\rho)$ inside the bisection method. When the evaluation of $\bar{S}(\rho)$ is fully distributed in the potential game $\mathcal{G}$, the complexity in each iteration of Algorithm 2 will be significantly reduced as each relay only requires to maximize a local objective in (13), with the solution readily given in (14). Finally, we observe that the relays requires information exchange between each other, i.e., each relay n requires $\boldsymbol{x}_{-n}$ and all channel information a_m to perform best response update as in (14), and the source also needs global information to update EH scheduling decision t as in lines 9-10 of Algorithm 2.

V. Simulation Results

In this section, we evaluate the proposed centralized and distributed algorithms through numerical experiments. We consider 3 relays located between a source and the destined receiver in two typical relay structures, namely, the isomorphic and heteromorphic structures as shown in Fig. 5. In isomorphic structure, relays are positioned similarly away from the source, while they are positioned very differently in the heteromorphic structure. Let $l_{A \to B}$ denote the distance between transceivers A and B. The mean path loss is given by $1/l_{A \to B}^e$ with the propagation exponent e set to 3.5. The channel gains are also subject to log-normal distributed random variables with zero mean and standard derivation 5dB [34]. In the simulation, we set $l_{S \to R_2} = l_{R_2 \to D} = 20m$ and $l_{R_1 \to R_2} = l_{R_2 \to R_3} = 5m$ in the isomorphic structure and the heteromorphic structure is a

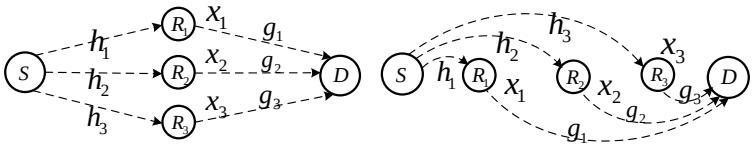

Fig. 5: Isomorphic (left) and heteromorphic (right) relay structures.

rotation of the isomorphic structure with the pivot at relay 2. The shortest source-relay distance in the heteromorphic structure is denoted by $l^H_{S\to R_1}$.

A. Comparison with Existing Relay Schemes

Firstly, we consider the isomorphic structure and compare throughput performance of the proposed centralized (optimal) and the distributed (sub-optimal) methods in Fig. 6. The global optimum, denoted by solid straight line in Fig. 6(a), is the performance upper bound achieved by the successive polyblock approximation in Algorithm 1. The distributed source-relay update method in Algorithm 2 decomposes the task of optimizing beamforming vector to N local sub-problems at individual relays. Initially, we set the relays' beamforming vector as $\boldsymbol{x} = [0.5, 0.5, 0.5]$ and EH scheduling decision as $t = 0.25$. We observe that Algorithm 2 iteratively converges to the global optimum as shown in Fig. 6(a). In the general case, we randomly generate relays' locations within a $15 \times 15m^2$ square area between the source and destination nodes. We record the throughput performance for 100 independent simulation runs and plot in Fig. 6(b) the relative performance difference between Algorithm 2 and its global optimum. All simulation results show that the distributed algorithm is almost as good as the centralized algorithm with no more than 0.2% performance loss. We also evaluate Algorithm 2 with an increasing number of relays and randomly generated initial values for $\boldsymbol{x} \in [\mathbf{0}, \mathbf{1}]$ and $t \in (0, \frac{1}{2})$. The comparison of the throughput performance between Algorithms 1 and 2 is shown in Table I. Row 2 of Table I shows the global optimal throughput r_1 obtained by Algorithm 1, which becomes larger with more collaborative relays. It also shows that the throughput performance of Algorithm 1 has very small difference with respect to the throughput r_2 obtained by Algorithm 2. Their relative differences are given in row 3 of Table I and generally less than 1% for different number of relays.

In Fig. 7, we compare the throughput performance of Algorithm 2 (denoted as Alg. 2 in Fig. 7) with some existing relay schemes, i.e., the max-min and greedy relay selection schemes

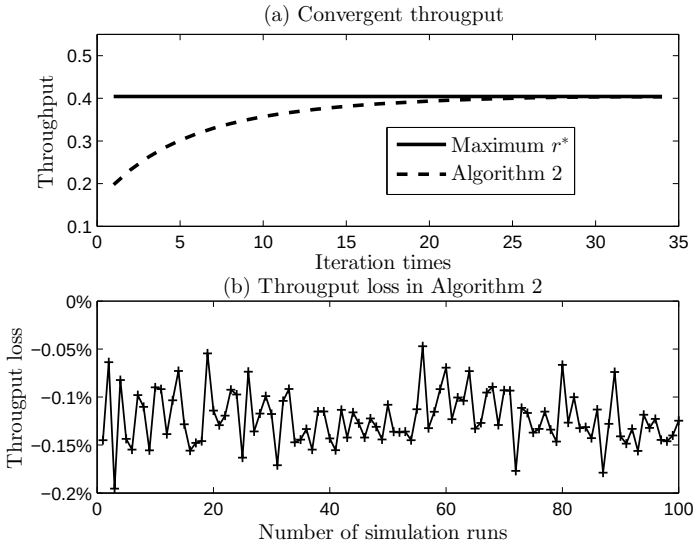

Fig. 6: Comparison of optimal and sup-optimal methods.

TABLE I: Comparison of optimal and sub-optimal methods

Number of Relays	$N = 4$	$N = 5$	$N = 6$	$N = 7$	$N = 8$
Thoughput r_1	0.87	1.03	1.14	1.20	1.33
$\frac{r_1 - r_2}{r_1} \times 100\%$	0.57%	0.51%	0.68%	0.69%	0.41%

in [15] as well as the optimal beamforming obtained in [18]. The max-min relay selection scheme first determines the worst link of the source-relay and relay-destination channels at each relay, i.e., $\ell_n = \min\{|h_n|^2, |g_n|^2\}$, then relay n^* with the strongest worst link is selected, i.e., $n^* = \max\{\ell_1, \ell_2, \ldots, \ell_N\}$. The greedy relay selection scheme chooses the relay n^* with the largest product of the source-relay and relay-destination channel gains, i.e., $n^* = \max\{|h_1|^2|g_1|^2, |h_2|^2|g_2|^2, \ldots, |h_N|^2|g_N|^2\}$. The results in Fig. 7(a) show that the proposed relay scheme in Algorithm 2 achieves significant throughput improvement compared with the single relay selection schemes. In the case of selecting multiple relays, the optimal beamforming vector is analytically obtained in [18] with fixed power supply at the relays. To compare it with our proposed relay scheme in Algorithm 2, we vary the EH time w that results in different power constraints at the relays, i.e., $p_n \leq \frac{c_n w}{(1-w)/2}$. For each fixed EH time w and rate $c \in \{1, 2, 3\}$, we apply the beamforming strategy in [18] and record the optimal throughput as shown by the curves in Fig. 7(b). The straight lines in Fig. 7(b) correspond to the optimal throughput achieved

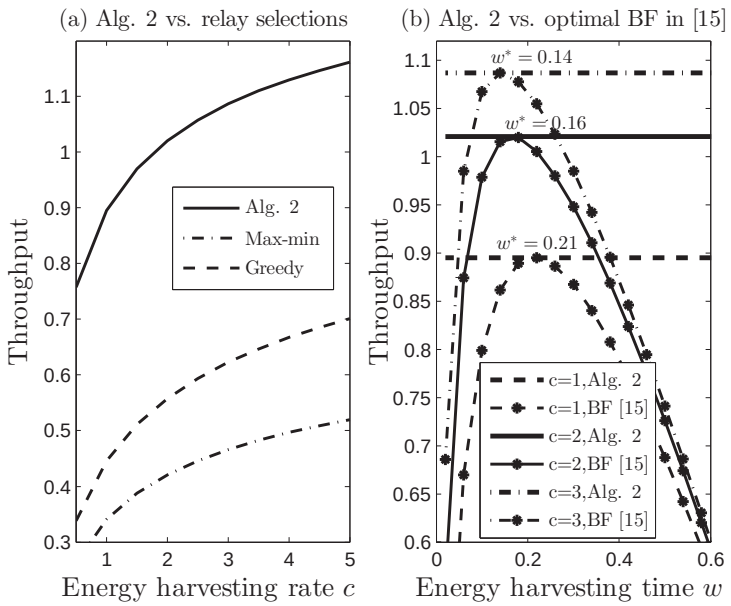

Fig. 7: Comparison with relay selection and beamforming schemes.

by Algorithm 2 with different EH time c. We observe that Algorithm 2 can obtain the maximum throughput by choosing the optimal EH time w^* as indicated in Fig. 7(b).

B. Relay Selection Driven by Source-Relay Link

Now we check how the throughput performance changes when all relays move away from the source in isomorphic structure. In this case, the source-relay channel h_n for each relay n is getting worse, while the relay-destination channel g_n is getting better. In Fig. 8(a), we plot the change of throughput with the same EH rate for all relays set to $c = 1$, $c = 3$, and $c = 5$, respectively. We observe from Fig. 8(a) that, a larger EH rate is always preferable as it increases the overall throughput, but the throughput improvement varies at different locations[5]. Specifically, when the relays move closer to the source ($l_{S\to R} \leq 20$), relays' EH profiles become the throughput bottleneck, thus the increase of EH rates will improve the throughput significantly. On the other hand, when the relays are far from source ($l_{S\to R} \geq 20$), the throughput can hardly change with respect to the increase of EH rates since the source-relay channels now become the performance

[5]We define the relay's location in terms of its distance to the source node (e.g., $l_{S\to R}$).

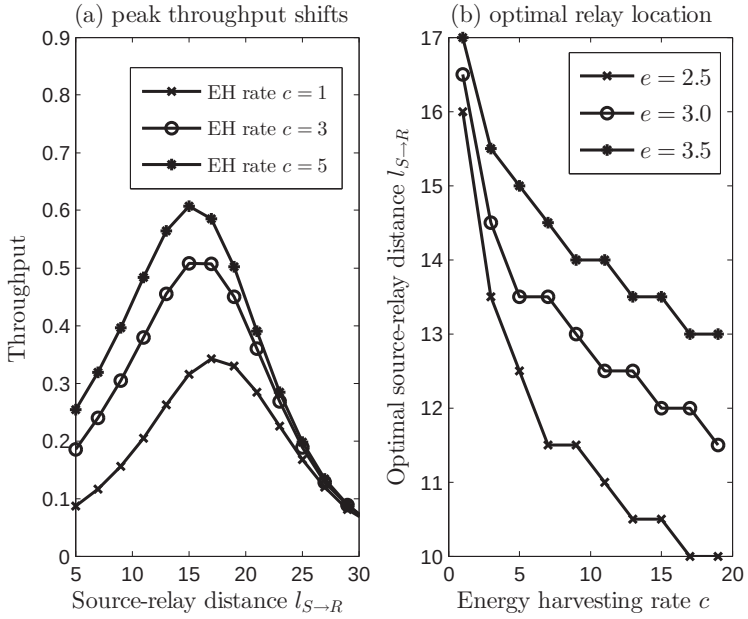

Fig. 8: Optimal relay locations shifts with varying EH rate c.

bottleneck. Therefore, the choice of relays should well balance the EH and channel profiles at individual relays.

Fig. 8(a) also shows that the maximum throughput is achieved when the relays are relatively close to the source. When the relays' EH rates increase, the optimal relay location is shifted toward the source, which implies that the source-relay channel is more important than the relay-destination channel for relays with energy harvesting constraints. This result is further shown in Fig. 8(b) where we plot the optimal relay's locations for different EH and channel conditions. The EH condition is represented by the EH rate in x-axis of Fig. 8(b) and the channel condition is denoted by different path loss exponent e in the legend of Fig. 8(b). A similar result can also be found for heteromorphic structure, while omitted here for conciseness.

C. Optimal Beamforming Vector at Relays

In this part, we study the throughput performance of the heteromorphic relay structure in Fig. 5 and compare it with the isomorphic structure. Fig. 9 plots their optimal throughput with different relays' EH rates. Starting from low EH rate, the isomorphic structure can better utilize the harvested energy of all relays, and thus contribute a higher throughput. When the EH rate

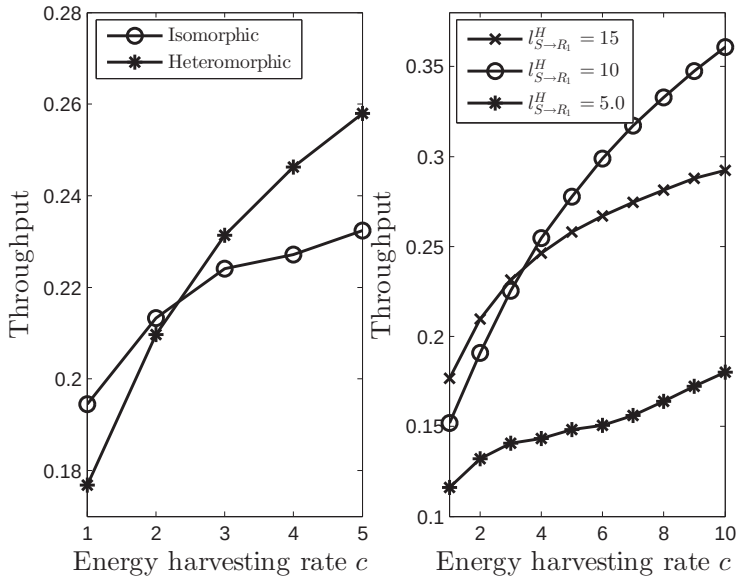

Fig. 9: Optimal throughput in different relay structures.

c increases, the relays can accumulate more energy and their channel conditions become the throughput bottleneck. Note that relay 1 in Fig. 5 has the shortest source-relay distance in heteromorphic structure, it has much better channel condition and thus can contribute to the most of the overall throughput. Therefore, we see a higher throughput in heteromorphic structure than that in isomorphic structure when EH rate is high, as shown in the left of Fig. 9. We further shift relay 1 closer to the source while keeping the same locations of relays 2 and 3, and plot the change of throughput with different source-relay distances in the right of Fig. 9. We observe that, the optimal throughput can be improved by properly shifting relay 1 to the source when EH rate is high, and shifting it away from source when EH rate is low. However, the overall throughput may drop significantly if relay 1 is too closer to the source, e.g., the case with $l_{S\to R_1}=5$. This is because, the throughput bottleneck is shifted from the source-relay to the relay-destination channel, i.e., though the source-relay channel is good and EH rate is high, relay 1 no longer contributes much to the overall throughput as the relay-destination channel deteriorates severely.

Fig. 10 shows the the relays' optimal beamforming vector $\boldsymbol{x}^*$ in the heteromorphic structure with different source-relay distances $l_{S\to R_1}$. As relay 1 always transmits with its peak power ($x_1=1$), we only show the power amplifier coefficients of the relays 2 and 3 in Fig. 10. We observe that, the relays' beamforming vector varies significantly according to the relays'

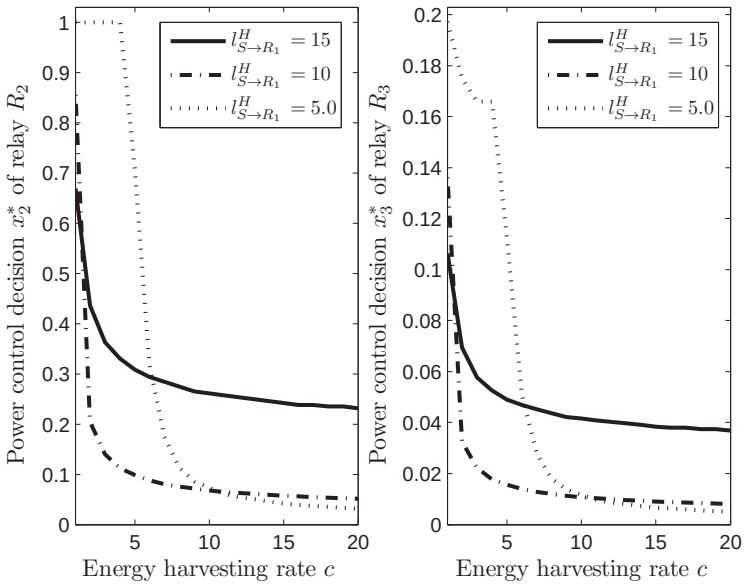

Fig. 10: Optimal power control decisions with different EH rates.

locations (or channel conditions), e.g., the small value of x_3^* shows that relay 3 is barely selected for transmission in either case due to its bad source-relay channel condition. We also find that, the relays' EH rate can significantly affect the power control decisions. When EH rate is low, relay 1 requires the help from the other relays to jointly improve the overall throughput. However, when EH rate is high, relay 1's contribution dominates the throughput performance, and the relays 2 and 3 are opting out of the relay network as shown in Fig. 10 where the power amplifier coefficients of relays 2 and 3 are decreasing very fast with the increase of EH rate.

VI. Conclusions

In this paper, we employ multiple relays powered by energy harvesting to forward data packets from a source to its destination. We study the interplay between EH and data transmission by formulating a throughput maximization problem that jointly optimizes EH scheduling and the relays' transmit power, by considering the variations of the relays' channel conditions and EH rates. We first propose a centralized scheme that achieves the global throughput by exploiting the monotonicity in the problem structure. We also propose a distributed sub-optimal scheme in a game theoretic approach that achieves near-optimal throughput performance. Simulation reveals some interesting results that may guide the choice and deployment of relays with EH constraints

in practice. Multi-hop relay network with EH constraints is one of our future research focuses. Variations in EH rates and channel conditions at different nodes further complicate the selection of relays and the routes for information forwarding. The accurate estimation of EH rates is also a challenging task and an active research area of our interest.

APPENDIX

A. Proof of Lemma 1

By the definition of normal set, we will show that, for any $\boldsymbol{z}^{(1)} = (t^{(1)}, \gamma^{(1)}) \succeq \boldsymbol{z}^{(2)} = (t^{(2)}, \gamma^{(2)}) \succeq 0$, we have $\boldsymbol{z}^{(2)} \in \Omega$ if $\boldsymbol{z}^{(1)} \in \Omega$. That is, we can find a solution $\boldsymbol{x}^{(2)} \in [\mathbf{0}, \mathbf{1}]$ such that $\gamma^{(2)} \leq \bar{\gamma}(t^{(2)}, \boldsymbol{x}^{(2)}) \triangleq \frac{(\boldsymbol{x}^{(2)})^T A \boldsymbol{x}^{(2)}}{f(t^{(2)}) + (\boldsymbol{x}^{(2)})^T B \boldsymbol{x}^{(2)}}$, given that $\gamma^{(1)} \leq \bar{\gamma}(t^{(1)}, \boldsymbol{x}^{(1)})$. Note that we have $f(t^{(2)}) = \frac{1}{1/t^{(2)} - 2} \leq \frac{1}{1/t^{(1)} - 2} = f(t^{(1)})$ if $t^{(2)} \leq t^{(1)}$. Thus, $\bar{\gamma}(t, \boldsymbol{x})$ is an decreasing function of t and we can always choose the same $\boldsymbol{x}^{(2)} = \boldsymbol{x}^{(1)}$ such that $\bar{\gamma}(t^{(2)}, \boldsymbol{x}^{(2)}) \geq \bar{\gamma}(t^{(1)}, \boldsymbol{x}^{(1)}) \geq \gamma^{(1)} \geq \gamma^{(2)}$, which implies that Ω is normal set.

If the optimum $\boldsymbol{z}^* = (t^*, \gamma^*)$ is not achieved on the upper boundary $\overline{\Omega}$, we can always find some $\boldsymbol{z}' = (t', \gamma') \in \overline{\Omega}$ and $\boldsymbol{z}' \succ \boldsymbol{z}^*$. Since $r(t, \gamma)$ is strictly increasing in both t and γ, we have $r(t', \gamma') > r(t', \gamma^*) > r(t^*, \gamma^*)$, which contradicts with the assumption.

B. Proof of Proposition 1

Lipschitz continuity requires that $||r(\boldsymbol{z}_2) - r(\boldsymbol{z}_1)|| \leq M||\boldsymbol{z}_2 - \boldsymbol{z}_1||$, $\forall \boldsymbol{z}_2, \boldsymbol{z}_1 \in \Omega$, where M is a constant. Let $\boldsymbol{z} = \boldsymbol{z}_1 + \theta(\boldsymbol{z}_2 - \boldsymbol{z}_1)$ and $g(\theta) = r(\boldsymbol{z})$, thus $g(0) = r(\boldsymbol{z}_1)$ and $g(1) = r(\boldsymbol{z}_2)$. By the fundamental theorem of calculus, we have $\Delta r \triangleq r(\boldsymbol{z}_2) - r(\boldsymbol{z}_1) = g(1) - g(0) = \int_\theta g'(\theta)\, d\theta$ and $g'(\theta) = \frac{\partial r(\boldsymbol{z})}{\partial \boldsymbol{z}}(\boldsymbol{z}_2 - \boldsymbol{z}_1)$, therefore we have

$$||\Delta r|| \leq \left|\left| \int_\theta \frac{\partial r(\boldsymbol{z})}{\partial \boldsymbol{z}}\, d\theta \right|\right| \cdot ||\Delta \boldsymbol{z}|| \leq \max \left|\left| \frac{\partial r(\boldsymbol{z})}{\partial \boldsymbol{z}} \right|\right| \cdot ||\Delta \boldsymbol{z}||.$$

Note that $\frac{\partial r(\boldsymbol{z})}{\partial \boldsymbol{z}} = \left[\log(1 + \gamma_1 + \theta(\gamma_2 - \gamma_1)), \frac{t_1 + \theta(t_2 - t_1)}{1 + \gamma_1 + \theta(\gamma_2 - \gamma_1)}\right]^T$, we can always set $M = ||[\log(1 + \gamma_{max}), 1/2]||$ such that $||r(\boldsymbol{z}_2) - r(\boldsymbol{z}_1)|| \leq M||\boldsymbol{z}_2 - \boldsymbol{z}_1||$, which shows that $r(t, \gamma)$ is Lipschitz continuous on Ω. Therefore, by Proposition 3.9 in [28], it is guaranteed to converge to ϵ-optimal solution within finite iterations.

C. Proof of Lemma 2

Firstly, note that $\lim_{t\to 0} r(t,\boldsymbol{x}) = 0$ and $\lim_{t\to 1/2} r(t,\boldsymbol{x}) = 0$. Thus, the optimal transmission time t is interior of $[0,1/2]$ as we can easily find a $t \in (0,1/2)$ such that $r(t,\boldsymbol{x}) > 0$. Concavity can be verified by checking the second derivative of $r(t,\boldsymbol{x})$ with respect to t as follows

$$\frac{\partial r}{\partial t} = \log(1+\gamma) + \frac{t}{1+\gamma}\frac{\partial \gamma}{\partial t}, \quad \text{and} \tag{15a}$$

$$\frac{\partial^2 r}{\partial t^2} = \frac{2}{1+\gamma}\frac{\partial \gamma}{\partial t} - \frac{t}{(1+\gamma)^2}\left(\frac{\partial \gamma}{\partial t}\right)^2 + \frac{t}{1+\gamma}\frac{\partial^2 \gamma}{\partial t^2}. \tag{15b}$$

Besides, we have $0 \geq \frac{\partial \gamma}{\partial t} = -\frac{\gamma}{(f(t)+\boldsymbol{x}^T B \boldsymbol{x})(1-2t)^2} \geq -\frac{\gamma}{t(1-2t)}$ and $\frac{\partial^2 \gamma}{\partial t^2} = \frac{\partial \gamma}{\partial t}\left(\frac{2}{\gamma}\frac{\partial \gamma}{\partial t} + \frac{4}{1-2t}\right)$, Substituting them into (15b), we get $\frac{\partial^2 r}{\partial t^2} = \frac{1}{1+\gamma}\frac{\partial \gamma}{\partial t}\left(\frac{2}{1-2t} + \frac{t(2+\gamma)}{\gamma(1+\gamma)}\frac{\partial \gamma}{\partial t}\right) \leq \frac{\gamma \partial \gamma/\partial t}{(1+\gamma)^2(1-2t)} \leq 0$, which verifies that the objective in (5) is strictly concave on $t \in (0,1/2)$. For any fixed beamforming vector $\boldsymbol{x}$, the best choice of t is always achieved at $\partial r(t,\boldsymbol{x})/\partial t = 0$.

D. Proof of Proposition 3

Suppose that the relay n unilaterally changes its power control parameter from x_n to $\bar{x}_n$, and then the strategy profile changes from $(x_n, \boldsymbol{x}_{-n})$ to $(\bar{x}_n, \boldsymbol{x}_{-n})$, we will check how the potential function $S(\boldsymbol{x},\rho)$ changes with the new strategy profile. We tear $S(\boldsymbol{x},\rho)$ into two parts, one relates to $\bar{x}_n$ and the other only relates to $\boldsymbol{x}_{-n}$ as follows:

$$\begin{aligned}
&S(x_n, \boldsymbol{x}_{-n}, \rho) \\
&= a_n^2 x_n \left(\left(1 - \frac{\rho}{h_n^2}\right) x_n + \sum_{m=1, m\neq n}^{N} \frac{a_m}{a_n} x_m + \sum_{k=1, k\neq n}^{N} \frac{a_k}{a_n} x_k \right) \\
&\quad + \sum_{k=1, k\neq n}^{N} a_k^2 x_k \left(\left(1 - \frac{\rho}{h_k^2}\right) x_k + \sum_{m=1, m\neq k, n}^{N} \frac{a_m}{a_k} x_m \right) \\
&= a_n^2 x_n \left(\left(1 - \frac{\rho}{h_n^2}\right) x_n + 2 \sum_{m=1, m\neq n}^{N} \frac{a_m}{a_n} x_m \right) \\
&\quad + \sum_{k=1, k\neq n}^{N} a_k^2 x_k \left(\left(1 - \frac{\rho}{h_k^2}\right) x_k + \sum_{m=1, m\neq k, n}^{N} \frac{a_m}{a_k} x_m \right) \\
&= u_n + \sum_{k=1, k\neq n}^{N} a_k^2 x_k \left(\left(1 - \frac{\rho}{h_k^2}\right) x_k + \sum_{m=1, m\neq k, n}^{N} \frac{a_m}{a_k} x_m \right).
\end{aligned}$$

Therefore, we have $S(x_n, \boldsymbol{x}_{-n}, \rho) - S(\bar{x}_n, \boldsymbol{x}_{-n}, \rho) = u_n(x_n, \boldsymbol{x}_{-n}) - u_n(\bar{x}_n, \boldsymbol{x}_{-n})$, which implies that $\mathcal{G}$ is an EPG with potential function $S(\boldsymbol{x}, \rho)$. Since $S(\boldsymbol{x}, \rho)$ is finite, relays' strategy updates will finally achieve a stable point at which $S(\boldsymbol{x}, \rho)$ cannot be improved any more, which corresponds to Nash equilibrium of the game $\mathcal{G}$.

E. Proof of Proposition 5

It is obvious that an all-ones vector $\mathbf{1}$ is the unique Nash equilibrium when all relays have good channel conditions. If all relays have bad channel conditions, the Nash equilibrium is a solution to a set of linear equations (i.e., $x_n = \beta_n \boldsymbol{a}_{-n}^T \boldsymbol{x}_{-n}$) projected on $[\mathbf{0}, \mathbf{1}]$, where $\boldsymbol{a}_{-n}$ is given in (3a) by removing the n-th element a_n. Therefore, either $\mathbf{0}$ or $\mathbf{1}$ would be unique Nash equilibrium depending on the coefficients $\beta_n \boldsymbol{a}_{-n}$. In the third case, at least one relay has good channel condition and owns the maximum power control parameter, say $x_n = 1$. Other relays' power control parameters are given by the intersections between hyperplanes $x_n = 1$ and $x_m = \beta_m \boldsymbol{a}_{-m}^T \boldsymbol{x}_{-m}$ for $m \neq n$, also projected on $[\mathbf{0}, \mathbf{1}]$.

For example, in a two-user case, relays' best response strategies can be represented by straight lines in a two dimensional space, e.g., $x_2 = \beta_2 \boldsymbol{a}_{-2}^T \boldsymbol{x}_{-2} = \beta_2 a_1 x_1$. The location of Nash equilibrium can be easily discussed according to the line slopes, which are given as $\beta_2 a_1$ and $\beta_1 a_2$, respectively according to (14). When $\beta_2 a_1 = \frac{1}{\beta_1 a_2}$, two best response curves collide with each other and any point on the curve becomes a Nash equilibrium. When $\beta_2 a_1 < \frac{1}{\beta_1 a_2}$, which is equivalent to $\rho > h_1^2 + h_2^2$, the best response iteration will converge to the unique fix point at $(0, 0)$, otherwise converge to $(1, 1)$ when $\rho < h_1^2 + h_2^2$. When $h_1^2 \geq \rho > h_2^2$, we simply have $x_1 = 1$ and $x_2 = (1, \min(\beta_2 a_1, 1))$.

REFERENCES

[1] S. Sudevalayam and P. Kulkarni, "Energy harvesting sensor nodes: Survey and implications," *IEEE Commun. Surveys Tuts.*, vol. 13, no. 3, pp. 443–461, Third 2011.

[2] R. Prasad, S. Devasenapathy, V. Rao, and J. Vazifehdan, "Reincarnation in the ambiance: Devices and networks with energy harvesting," *IEEE Commun. Surveys Tuts.*, vol. 16, no. 1, pp. 195–213, First 2014.

[3] J. Yang and S. Ulukus, "Optimal packet scheduling in an energy harvesting communication system," *IEEE Trans. Commun.*, vol. 60, no. 1, pp. 220–230, Jan. 2012.

[4] K. Tutuncuoglu and A. Yener, "Optimum transmission policies for battery limited energy harvesting nodes," *IEEE Trans. Wireless Commun.*, vol. 11, no. 3, pp. 1180–1189, Mar. 2012.

[5] C. Huang, R. Zhang, and S. Cui, "Throughput maximization for the Gaussian relay channel with energy harvesting constraints," *IEEE J. Sel. Areas Commun.*, vol. 31, no. 8, pp. 1469–1479, Aug. 2013.

[6] J. Xu and R. Zhang, "Throughput optimal policies for energy harvesting wireless transmitters with non-ideal circuit power," *IEEE J. Sel. Areas Commun.*, vol. 32, no. 2, pp. 322–332, Feb. 2014.

[7] N. Gautam and A. Mohapatra, "Efficiently operating wireless nodes powered by renewable energy sources," *IEEE J. Sel. Areas Commun.*, vol. 33, no. 8, pp. 1706–1716, Aug. 2015.

[8] I. Ahmed, A. Ikhlef, D. Ng, and R. Schober, "Power allocation for an energy harvesting transmitter with hybrid energy sources," *IEEE Trans. Wireless Commun.*, vol. 12, no. 12, pp. 6255–6267, Dec. 2013.

[9] N. Michelusi, K. Stamatiou, and M. Zorzi, "Transmission policies for energy harvesting sensors with time-correlated energy supply," *IEEE Trans. Commun.*, vol. 61, no. 7, pp. 2988–3001, Jul. 2013.

[10] D. Gunduz, K. Stamatiou, N. Michelusi, and M. Zorzi, "Designing intelligent energy harvesting communication systems," *IEEE Commun. Mag.*, vol. 52, no. 1, pp. 210–216, Jan. 2014.

[11] A. Nasir, X. Zhou, S. Durrani, and R. Kennedy, "Relaying protocols for wireless energy harvesting and information processing," *IEEE Trans. Wireless Commun.*, vol. 12, no. 7, pp. 3622–3636, Jul. 2013.

[12] Z. Ding, S. Perlaza, I. Esnaola, and H. Poor, "Power allocation strategies in energy harvesting wireless cooperative networks," *IEEE Trans. Wireless Commun.*, vol. 13, no. 2, pp. 846–860, Feb. 2014.

[13] K. Tutuncuoglu and A. Yener, "Cooperative energy harvesting communications with relaying and energy sharing," in *Proc. IEEE Information Theory Workshop (ITW)*, Sep. 2013.

[14] I. Ahmed, A. Ikhlef, R. Schober, and R. Mallik, "Joint power allocation and relay selection in energy harvesting AF relay systems," *IEEE Wireless Commun. Lett.*, vol. 2, no. 2, pp. 239–242, Apr. 2013.

[15] Z. Ding and H. V. Poor, "Energy harvesting cooperative networks: Is the max-min criterion still diversity-optimal?" *CoRR*, vol. abs/1403.0354, 2014. [Online]. Available: http://arxiv.org/abs/1403.0354

[16] B. Medepally and N. Mehta, "Voluntary energy harvesting relays and selection in cooperative wireless networks," *IEEE Trans. Wireless Commun.*, vol. 9, no. 11, pp. 3543–3553, Nov. 2010.

[17] J. M. Gilbert and F. Balouchi, "Comparison of energy harvesting systems for wireless sensor networks," *International Journal of Automation and Computing*, vol. 5, no. 4, pp. 334–347, 2008.

[18] Y. Jing and H. Jafarkhani, "Network beamforming using relays with perfect channel information," *IEEE Trans. Inf. Theory*, vol. 55, no. 6, pp. 2499–2517, Jun. 2009.

[19] B. Bejar Haro, S. Zazo, and D. Palomar, "Energy efficient collaborative beamforming in wireless sensor networks," *IEEE Trans. Signal Process.*, vol. 62, no. 2, pp. 496–510, Jan. 2014.

[20] I. Krikidis, G. Zheng, and B. Ottersten, "Harvest-use cooperative networks with half/full-duplex relaying," in *Proc. IEEE WCNC*, Apr. 2013, pp. 4256–4260.

[21] M.-Y. Cheng, Y.-B. Chen, H.-Y. Wei, and W. Seah, "Event-driven energy-harvesting wireless sensor network for structural health monitoring," in *Proc. IEEE Local Computer Networks (LCN)*, Oct. 2013, pp. 364–372.

[22] X. Lu, P. Wang, D. Niyato, D. I. Kim, and Z. Han, "Wireless networks with rf energy harvesting: A contemporary survey," *IEEE Commun. Surveys Tuts.*, vol. PP, no. 99, pp. 1–35, 2015.

[23] F. Gao, R. Zhang, and Y.-C. Liang, "Channel estimation for ofdm modulated two-way relay networks," *IEEE Trans. Signal Proces.*, vol. 57, no. 11, pp. 4443–4455, Nov. 2009.

[24] F. Iannello, O. Simeone, and U. Spagnolini, "Medium access control protocols for wireless sensor networks with energy harvesting," *IEEE Trans. Commun.*, vol. 60, no. 5, pp. 1381–1389, May 2012.

[25] D. Gunduz and B. Devillers, "Two-hop communication with energy harvesting," in *Proc. IEEE International Workshop on Computational Advances in Multi-Sensor Adaptive Processing (CAMSAP)*, Dec. 2011, pp. 201–204.

[26] Y. Luo, J. Zhang, and K. Letaief, "Optimal scheduling and power allocation for two-hop energy harvesting communication systems," *IEEE Trans. Wireless Commun.*, vol. 12, no. 9, pp. 4729–4741, Sep. 2013.

[27] L. Feeney and M. Nilsson, "Investigating the energy consumption of a wireless network interface in an ad hoc networking environment," in *Proc. IEEE INFOCOM*, vol. 3, 2001, pp. 1548–1557.

[28] Y. J. A. Zhang, L. Qian, and J. Huang, "Monotonic optimization in communication and networking systems," *Foundations and Trends in Networking*, vol. 7, no. 1, pp. 1–75, 2013.

[29] J. B. Lasserre, "Global optimization with polynomials and the problem of moments," *SIAM Journal on Optimization*, vol. 11, pp. 796–817, 2001.

[30] J. Gotoh and H. Konno, "Maximization of the ratio of two convex quadratic functions over a polytope," *Computational Optimization and Applications*, vol. 20, no. 1, pp. 43–60, 2001.

[31] W. Dinkelbach, "On nonlinear fractional programming," *Management Science*, vol. 13, no. 7, pp. 492–498, 1967.

[32] D. Monderer and L. Shapley, "Potential games," *Games and Economic Behavior*, vol. 14, no. 1, pp. 124–143, 1996.

[33] Y. Nesterov and A. Nemirovskii, *Interior-Point Polynomial Algorithms in Convex Programming*. Society for Industrial and Applied Mathematics, 1994.

[34] S. Gong, P. Wang, Y. Liu, and W. Zhuang, "Robust power control with distribution uncertainty in cognitive radio networks," *IEEE J. Sel. Areas Commun.*, vol. 31, no. 11, pp. 2397–2408, Nov. 2013.